



Nanoelectrical and Nanoelectrochemical Imaging of Pt/p-Si and Pt/p⁺-Si Electrodes

Jingjing Jiang^{+, [a]}, Zhuangqun Huang^{+, [b]}, Chengxiang Xiang,^[c] Rakesh Poddar,^[b] Hans-Joachim Lewerenz,^[a] Kimberly M. Papadantonakis,^[c] Nathan S. Lewis,^{*, [c, d]} and Bruce S. Brunshwig^{*, [d]}

The interfacial properties of electrolessly deposited Pt nanoparticles (Pt-NPs) on p-Si and p⁺-Si electrodes were investigated on the nanometer scale using a combination of scanning probe methods. Atomic force microscopy (AFM) showed highly dispersed Pt-NPs with diameters of 20–150 nm on the Si surface. Conductive AFM measurements showed that only approximately half of the particles exhibited measurable contact currents, with a factor of 10³ difference in current observed between particles at a given bias. Local current–voltage measurements revealed a rectifying junction with a resistance ≥ 10 M Ω at the Pt-NP/p-Si interface, whereas the Pt-NP/p⁺-Si samples formed an ohmic junction with a local resistance ≥ 1 M Ω . The particles were strongly attached to the sample surface in air. However, in an electrolyte, the adhesion of the particles to the

surface was substantially lower, and most of the particles had tip-contact currents that varied by a factor of approximately 10. Scanning electrochemical microscopy (SECM) showed smaller but more uniform electrochemical currents for the particles relative to the currents observed by conductive AFM. In accord with the conductive AFM measurements, the SECM measurements showed conductance through the substrate for only a minority of the particles. These results suggest that the electrochemical performance of the electrolessly deposited Pt nanoparticles on Si can be ascribed to: 1) The high resistance of the contact between the particles and the substrate, 2) the low (<50%) fraction of particles that support high currents, and 3) the low adhesion of the particles to the surface when in contact with the electrolyte.

Introduction

Photoelectrochemical (PEC) water-splitting systems place catalysts for the water-splitting half-reactions in electrical contact with semiconducting photoelectrodes that convert light energy into separated positive and negative charges.^[1–3] In such systems, the interfaces between the light absorbers and

catalysts must provide a robust mechanical attachment of the catalyst to the surface as well as a pathway for the charge to flow from the light absorber to the catalyst.

Electroless plating is a widely used method for the deposition of metal catalysts onto photoelectrodes.^[4] Kulkarni and co-workers summarized the history of electroless deposition methods, including optimization of plating conditions (e.g., concentration, pH, temperature), particle density on the surface, and proposed particle-growth mechanisms.^[5]

Pt/Si interfaces show different electron transport behavior for hydrogen production when Pt is deposited electrolessly relative to when Pt is deposited by electron-beam evaporation.^[4d] X-ray photoelectron spectroscopy (XPS) indicated the formation of Si oxide at the interface between the electrolessly deposited particles and the Si substrate, whereas no interfacial Si oxide was observed for evaporated Pt.^[4d] Furthermore, weak adhesion of some metals films and nanoparticles (NPs) to Si surfaces with SiO₂ layers was observed.^[6]

The present understanding of interfaces between Pt-NPs and Si substrates is primarily derived from macroscopic measurements, as opposed to methods that provide information about the electrical and electrochemical properties of individual NPs.^[7,8]

We describe herein the electrical and mechanical properties of individual electrolessly deposited Pt-NPs on Si(111) surfaces as measured using atomic-force microscopy (AFM). The electrical and mechanical properties were measured both in air and

[a] J. Jiang,⁺ Dr. H.-J. Lewerenz
Division of Engineering and Applied Science
California Institute of Technology
Pasadena, CA 91125 (USA)

[b] Dr. Z. Huang,⁺ Dr. R. Poddar
Bruker Nano Surfaces
112 Robin Hill Road, Goleta, CA 93117 (USA)

[c] Dr. C. Xiang, Dr. K. M. Papadantonakis, Prof. N. S. Lewis
Division of Chemistry and Chemical Engineering
California Institute of Technology
Pasadena, CA 91125 (USA)

[d] Prof. N. S. Lewis, Dr. B. S. Brunshwig
Beckman Institute
California Institute of Technology
Pasadena, CA 91125 (USA)
E-mail: nslewis@caltech.edu
bsb@caltech.edu

[⁺] These authors contributed equally to this work.

Supporting Information and the ORCID identification number(s) for the author(s) of this article can be found under:
<https://doi.org/10.1002/cssc.201700893>.

This publication is part of a Special Issue on the topic of Artificial Photosynthesis for Sustainable Fuels. To view the complete issue, visit:
<http://dx.doi.org/10.1002/cssc.v10.22>.

in contact with an electrolyte. The surface topography and conductivity of electrolessly deposited Pt-NPs were simultaneously imaged by AFM. The force needed to move the particles on the surface was measured, and the area under the particles was examined. Furthermore, the conductance of the particles in contact with an electrolyte was mapped using AFM-based scanning electrochemical microscopy (SECM).

Results and Discussion

Topography and conductivity of Pt/p-Si in air

Figures 1 and S1 (Supporting Information) show the AFM topography and conductivity data for a Pt-NP/p-Si electrode prepared using electroless Pt deposition. Figure 1A shows a typical scan of the Pt/p-Si sample. Analysis of multiple scans indicated that the width of the particles varied between approximately 20–150 nm, whereas the height of the particles was between approximately 20–250 nm. Figure 1B and C show contact currents measured at sample biases of 0.3 and –0.3 V, respectively. The magnitudes of the currents were asymmetric with respect to the sign of the applied voltage. For example, at 0.3 V, the contact currents varied from the detection limit of <1 pA to 10³ pA (Figure S1), whereas at –0.3 V, the reverse current ranged from ≤1 to 10 pA. No apparent correlation was observed between the contact currents at the two voltages (Figure 1D, solid blue line at 0.3 V vs. dotted red line at –0.3 V), and little apparent correlation was observed between the current and the surface height (dashed green line). Only

approximately half of the particles exhibited contact currents that were above the detection limit. For example, the topographic line profile shown in Figure 1 crossed ten nanoparticles, but only five particles exhibited measurable currents (>2 pA) when the sample was biased at 0.3 V.

The current–voltage (*I*–*V*) data measured for individual particles showed rectifying behavior; however, the *I*–*V* behavior under forward bias varied substantially between particles. For particles located at positions 1, 2, and 3 (Figure 1B), the currents started rising at approximately 0, 0.1, and 0.3 V, respectively. No nanoparticle was present at location 4, and negligible current (–1.8 to –1.4 pA) was measured at this location.

The *I*–*V* data of particles 1–3 (Figure 1B) were fitted to the thermionic emission equation [Eq. (1)] considering a series resistance in the circuit:

$$I(V) = AA^* T^2 e^{\left(\frac{-q\varphi_B}{k_B T}\right)} \left[e^{\left(\frac{q(V-IR)}{nk_B T}\right)} - 1 \right] \quad (1)$$

in which *I*(*V*) is the current at voltage *V* relative to the equilibrium voltage; *A* is the junction contact area; *A** is the effective Richardson's constant (1.2 × 10⁶ Am^{–2} K^{–2});^[9] *T* is the absolute temperature, *q* is the unsigned charge of an electron, *k*_B is Boltzmann's constant; φ_B is the barrier height, *n* is the ideality factor, and *R* is the resistance of the sample. Fitted results are plotted as solid lines in Figure 1E, and the fitted values of φ_B , *n*, and *R* are listed in Table 1. The particles had barrier heights of approximately 0.55 V with resistances of 12–60 MΩ.

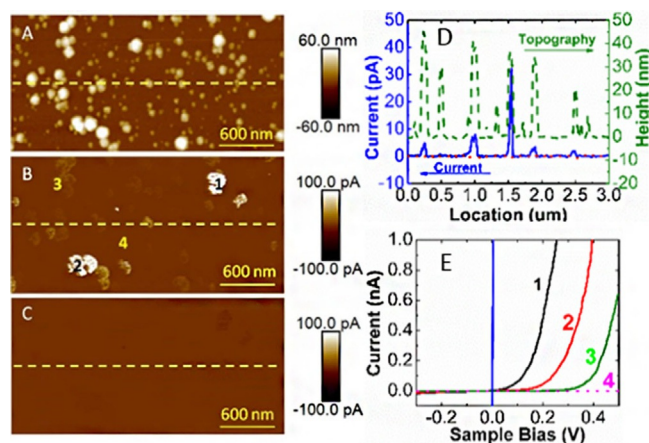


Figure 1. Topography, conductivity, and *I*–*V* spectroscopy of Pt nanoparticles electrolessly deposited onto a p-Si substrate and measured in air. (A) Surface topography, (B) and (C) contact currents shown for sample biases of 0.3 and –0.3 V, respectively. (D) Cross-sectional analysis of the surface topography (dashed green line), contact current at 0.3 V (solid blue line), and –0.3 V (dotted red line) sample biases for the portion of the sample indicated by the dashed yellow line in (A), (B), and (C). The left and right ordinates are the contact current and surface topography, respectively. (E) Point-specific *I*–*V* characteristics for the locations corresponding to the labels in (B). The vertical blue curve is an *I*–*V* measurement from a Pt thin film deposited onto p-Si by electron-beam evaporation. The solid lines for curves 1–3 in E are fits to equation 1, whereas the blue solid line is a fit to Ohm's law. The fitted curves match well with the experimental curves. Nanoparticles were present at positions 1, 2, and 3, but no nanoparticle was present at location 4.

Table 1. Results from fitting the *I*–*V* data for particles 1–3 to the thermionic emission equation with a series resistor [Eq. (1)]. Parameters are described in the text. The *I*–*V* data of the Pt thin film/p-Si was fitted to Ohm's law. N/A = not available.

Particle	φ_B [eV]	<i>n</i>	<i>R</i> [MΩ]
1	0.53	1.5	49
2	0.52	2.6	12
3	0.57	1.4	63
thin film	N/A	N/A	3

Figures 1E and S2 show the *I*–*V* characteristics of a Pt thin film/p-Si (Pt-TF/p-Si) sample prepared using electron-beam evaporation. The data were spatially uniform, indicating that the deposition resulted in a homogenous metal thin film. A linear response was observed within the range of the voltage scan (Figure S2), with a resistance of 3 MΩ for the measured contact area. A much larger current was observed for the Pt-TF/p-Si sample than for the samples prepared using electroless Pt deposition.

The results presented in Figure 1 were qualitatively similar for several replicate samples. For example, Figure S3 shows results from a different sample that was prepared following nominally the same procedures as that for the sample displayed in Figure 1. Both the 2D images as well as the 3D topographic images showed a highly dispersed distribution of particle sizes and a range of currents that spanned thousands of pA.

Topography and conductivity of Pt/ p⁺-Si in air

Conductivity imaging and local *I*-*V* spectroscopy by PeakForce Tunneling AFM (PF-TUNA) was also performed on Pt/p⁺-Si electrodes made from either electrolessly deposited Pt nanoparticles or by electron-beam deposition of a Pt thin film. The size and height distributions for the particles from analysis of multiple scans were approximately 20–150 nm and 30–300 nm, respectively, on a Pt-NP/p⁺-Si sample (Figure 2A), similar to those observed for the Pt-NP/p-Si sample. As shown in Figure 2B, only approximately one third of the particles showed conductive contrast on a 5 nA scale. The contact currents ranged from approximately 10 pA (for a particle not evident in the topographic image) to approximately 50 nA (a factor of 10³ larger than for Pt-NP/p-Si). Figure 2C shows *I*-*V* data for the locations labeled in Figure 2A. Particles 1 and 2 showed relatively ohmic behavior in this measurement window, with resistances of 1.5 and 26 MΩ, respectively, between -50 and 50 mV. A Pt-TF/p⁺-Si sample showed location-independent ohmic *I*-*V* data with a resistance of 2 kΩ.

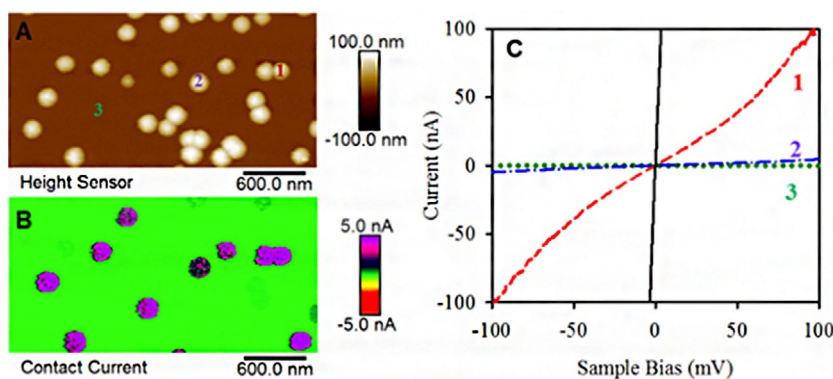


Figure 2. Topography, conductivity, and *I*-*V* spectroscopy of Pt nanoparticles electrolessly deposited onto a degenerately doped p⁺-Si substrate and captured by PF-TUNA in air. (A) Surface topography and (B) contact currents for a sample bias of 0.1 V. (C) Point-specific *I*-*V* characteristics at locations corresponding to the labels on (A); Nanoparticles were present at location 1 and 2 whereas no particle was present at location 3. An *I*-*V* plot for a sample with a thin film of Pt prepared by electron-beam evaporation on p⁺-Si is also shown (black solid line).

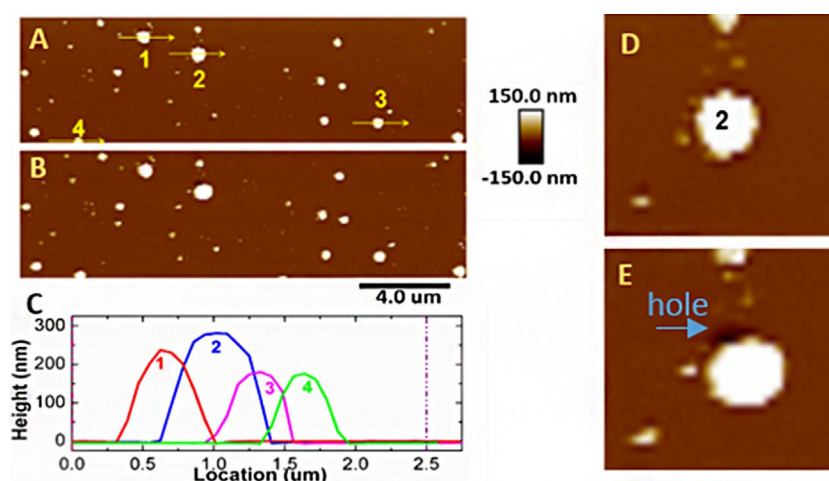


Figure 3. (A) Surface topography for a sample area imaged by classic tapping mode in air before the pushing process. The yellow arrows and numerical labels indicate the four particles subjected to pushing from left to right by the probe tip. (B) Surface topography of the same area in (A) imaged by classic tapping mode in air after the pushing process; and (C) line profiles of the four particles indicated in (A). From left to right are particle 1 (red line), 2 (blue line), 3 (pink line), and 4 (green line). Zoomed-in views of particle 2 (D) before and (E) after pushing.

Adhesion for Pt-NP/p⁺-Si in air

A TESPA probe (Bruker) was used to evaluate the adhesion of the particles to the substrate. The probe had a nominal spring constant of 40 N m⁻¹, approximately 20 times higher than that of the SECM probe (2.2 N m⁻¹) used below. During the pushing process, a particle was first locally detected using conventional tapping mode. The tip oscillation was stopped and then the tip was held 10 nm above the surface while moving from left to right across a particle by more than 1 μm. Particles subjected to pushing had heights of > 150 nm.

Figure 3A and B present the surface topography for an area of the sample before and after the particle-pushing process for samples in contact with air. From the comparison, only particle 2 was moved by the force from the tip. Particle 2 was the tallest particle (≈ 275 nm) for which pushing was attempted, and after particle 2 was moved, a small hole (200 nm width and 50 nm depth) was observed on the top left adjacent to the particle. For particles that remained in position, contact by the cantilever during the pushing attempt resulted in bending

of the cantilever > 100 nm, corresponding to a force of > 4 μN . This contact force would be expected to dull the tip. An approximately 10% increase in the mean apparent particle diameter was observed after pushing, consistent with dulling of the probe tip (Table S1).

Adhesion to Pt-NP/ p^+ -Si in electrolyte

Figure 4 shows the topography of an electrode surface in contact with 0.1 M KCl(aq), as measured during a PF-SECM scan using an imaging force of 2.8 nN. The white arrows in Figure 4A and 4B indicate the slow-scanning direction for the 5×5 μm scan area. The scan rate of 1 Hz corresponded to a horizontal tip velocity of $10 \mu\text{m s}^{-1}$. The SECM image was captured following a PeakForce Tapping (PFT) line scan on the retrace cycle (right to left scan) during the lift mode. The Pt particles were swept away from their original locations during the prior PFT line scan, and were observed only in the upper-left-hand half of the image. A subsequent bottom-to-top scan showed particles only in the top left-hand corner of the scanning area (Figure 4B). High-resolution topographic imaging within the original scan area showed indentations in the Si surface after the SECM scan, where the particles were located originally, inferred from the size and distribution of the holes, and the particles were pushed to the edges of the surface. The depressions had depths between 0.2 and 0.8 nm and showed a variety of in-hole structures. Figure S4 shows the cross-sectional analysis of a typical hole, which exhibited a width and depth of approximately 150 and 0.7 nm, respectively.

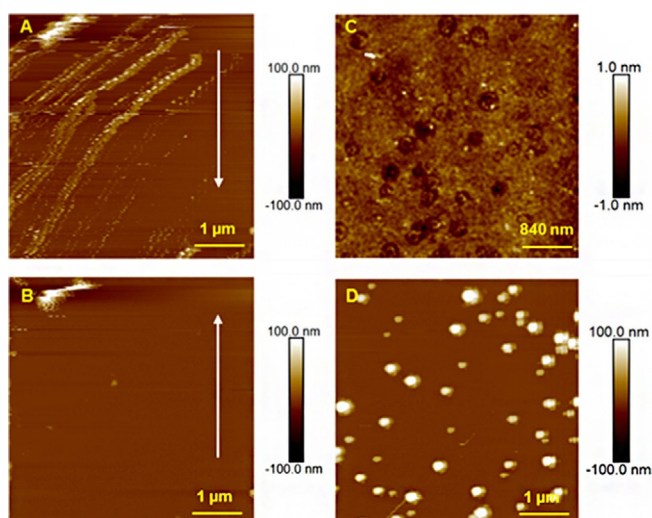


Figure 4. Topography of electrolessly deposited Pt nanoparticles on a degenerately doped p^+ -Si substrate as measured by PF-SECM using a SECM probe. (A) Retrace (right to left scanning) image of the surface topography in 0.1 M KCl at an imaging force of 2.8 nN with a slow scanning direction from top to bottom, and (B) the subsequent bottom-to-top scan. The tip velocity was $10 \mu\text{m s}^{-1}$. (C) Surface topography of the featureless area in (B) showing depressions in the surface in which the particles were located before they were moved by the SECM probe. (D) Surface topography of a different area of the same electrode imaged in air at an imaging force of 4.3 nN after being vigorously rinsed with H_2O and dried under N_2 .

After SECM imaging of the sample in contact with the aqueous electrolyte, the sample was vigorously rinsed with a large quantity of water, dried under flowing $\text{N}_2(\text{g})$, and reimaged. Using the same SECM probe, a different area of the sample was examined in air with an imaging force of 4.3 nN, similar to the 5 to 10 nN force used by the PF-TUNA scans in air. The surface topography (Figure 3D) was similar to the Pt-NP/ p^+ -Si surface image in air obtained previously (Figure 2A). The sample was then soaked in 0.1, 0.5, and 1.0 M KCl(aq) for 2 h, rinsed with water, dried with $\text{N}_2(\text{g})$, and imaged again. These images indicated that the particles were not moved by the SECM probe when the surface was mapped in air.

SECM of Pt-NP/ p^+ -Si in electrolyte

The nanoelectrode SECM probe had a conical tip with an exposed active tip end that was approximately 50 nm in diameter and 250 nm in height.^[10] Figure S5A shows two cyclic voltammograms (CVs) for the probe used in the imaging, with the sigmoidal shape typical of a nanoelectrode. To confirm that the measured current originated from the tip apex rather than the sides of the tip, the approach curve of the nanoelectrode probe was measured over a particle-free region of the Pt/ p^+ -Si electrode (Figure S5B) while the tip was biased at -0.4 V versus Ag wire as a quasi-reference electrode (AgQRE) to obtain a diffusion-limited current. The tip current decreased from 1.38 nA at a tip-sample distance of $1 \mu\text{m}$ to 1.05 nA when the tip was at the sample surface. The 25% reduction in current is consistent with simulations reported in previous work.^[10]

A very low imaging force (700 pN) and small tip velocity ($1.2 \mu\text{m s}^{-1}$) were used to obtain PF-SECM measurements on a Pt-NP/ p^+ -Si substrate while minimizing movement of particles under the electrolyte. Figure 5A and Figures S6 and S7 show the surface topography in an area in which particles of sizes 20

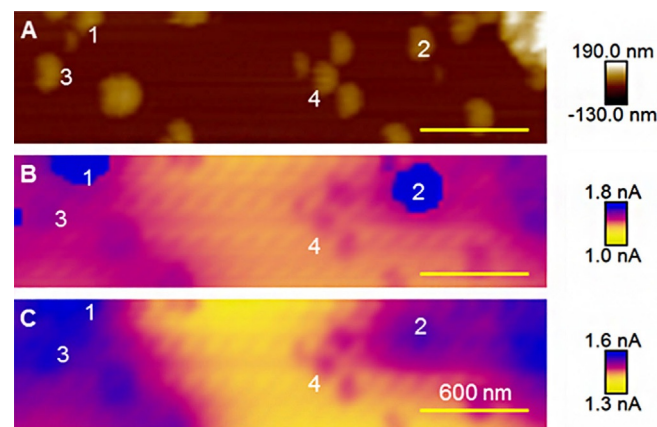


Figure 5. PF-SECM imaging of Pt nanoparticles electrolessly deposited onto a degenerately doped p^+ -Si substrate and in contact with 10 mM $[\text{Ru}(\text{NH}_3)_6]^{3+}$ and 0.1 M KCl(aq) with an imaging force of 700 pN and a tip velocity of $1.2 \mu\text{m s}^{-1}$. The nanoelectrode probe and the sample were biased at -0.4 V and -0.1 V vs. a AgCl-coated AgQRE, respectively. A $3 \mu\text{m} \times 750$ nm area was scanned. (A) Surface topography. (B) Tip-contact current captured during the main PFT scan. (C) Electrochemical current captured during the lift scan at a lift height of 150 nm. The scale bar is 600 nm.

to 250 nm were observed. The heights of these particles were between 30–100 nm. Figure 5B shows the tip-contact current obtained from the main scan during the SECM imaging. These tip-contact currents had a distribution from approximately 1.37 nA for the background signal on a flat Si area to approximately 7 nA on particle 2. Except for particles at locations 1 and 2 (Figure 5B), the tip-contact currents for all the other particles were < 1.6 nA (Figure S6). Region 4 was a cluster of four nanoparticles close together with sizes of approximately 120 × 180 nm. The tip-contact-current map barely differentiated between these four particles, as shown in Figure 5B.

Figure 5C shows the SECM current measured during the lift scans while a tip-to-sample distance of 100 nm was maintained. The SECM current map, much like the tip-contact-current map, showed a more convoluted surface than the current maps in air, as evidenced by a comparison of Figures S1 and S3 with Figure S6. This behavior was in part owing to the Faradaic current observed even when the tip was in contact with an electrochemically inactive area of the surface. The SECM current near the center of the image was approximately 1.40 nA. For particles in region #4, the SECM current increased by approximately 50 pA, whereas the current increased by approximately 0.18, 0.14, and 0.17 nA for particles at locations 1, 2, and 3, respectively. The electrochemical imaging resolved particles in region 4. These correlated maps allowed comparison between the surface topography, contact current, and SECM faradaic current for the different particles. For example, regions 2 and 3 had particles with sizes of approximately 120 × 200 nm and a height of approximately 65 nm, but particle at location 2 had a tip-contact current approximately five times larger than that of particle at location 3 and exhibited an SECM current approximately 20% less than particle at location 3.

Discussion

PtCl₆²⁻ and PtCl₄²⁻ are strong oxidants ($E^0 \approx 0.7$ V vs. normal hydrogen electrode (NHE) for the PtCl₆²⁻/PtCl₄²⁻ and PtCl₄²⁻/Pt couples). Thermodynamically, these metal cations can oxidize Si and in the presence of water SiO₂ can form on the surface [Eq. (2)].



Because metal deposition is hindered by the presence of SiO₂ on the Si surface, HF(aq) was added to the deposition solution to remove the SiO₂, [Eq. (3)]. However, the oxide under the Pt nanoparticles was not completely removed.^[4d] The data reported herein underscore the impact on the interfacial conductivity and energetics of this interfacial oxide layer between the Si and the Pt particles.

The electron affinity of bulk Si(111) has been estimated to be 4.05 eV^[11] and the Si band gap is 1.12 eV. Thus, under flat-band conditions, the valance-band edge of Si is located at a potential of 5.17 V versus vacuum.^[11] Pt has a work function of approximately 5.6 eV,^[12] thus, the band positions suggest that an

ideal Pt/Si contact would be ohmic, as is generally observed for p-Si.^[9] The rectifying behavior observed on the nanoparticle samples can thus be attributed to the interfacial Pt-NP/Si junction, which produces a resistive diode-like junction. Although a resistive junction is not desired for kinetic reasons (current), the observed high barrier height owing to the rectifying junction benefits the energetics (photovoltage).

The Pt-NP/p⁺-Si samples yielded ohmic behavior, as expected for two metallic materials in contact, even if a thin oxide layer existed at the interface. The Pt-NP/p⁺-Si junction was more conductive locally than the Pt-NP/p-Si junction (1.4–26 vs. 10–60 MΩ), similar to observations for the Pt-TF/p-Si. The high resistances observed for the particles may be due in part to the SiO₂ layer between the silicon and the Pt-NPs.

The mechanical adhesion is not robust between a Pt thin film and Si. Consequently, an interfacial adhesion layer is normally required when Pt is deposited by physical vapor deposition onto Si substrates. For a Pt thin film deposited directly on Si, imaging forces of < 10 nN did not damage the surface in air. The Pt-NP/Si sample showed strong mechanical attachment of the particles to the substrate in air, and even a stiff cantilever did not push the particles away from the surface. However, the adhesion changed substantially in aqueous solution; under such conditions, intermittent contact imaging with a force < 1/20th of that used in air pushed the Pt nanoparticles out of the imaging scan. The presence of an electrolyte may change the interfacial energetics at the semiconductor/metal junctions,^[13] and such changes may be owed to the change of interfacial mechanics.

Movement of the particles on the surface allows study of the surface of the substrate that was originally beneath the particle. The metal particles were partially embedded into the Si surfaces (Figures 4 and S4),^[8,14] and the surface indentations varied, typically < 1 nm in depth.

Although only loosely attached to the Si surface when in contact with an electrolyte, currents were passed through the particles, with some particles supporting high current densities. For example, the tip-contact current depicted in the SECM scans of Figures 5B and S7 was > 7 nA for particle 2. While the tip was in contact with the particle for only part of the tapping cycle, the tip-contact current was averaged over the full cycle. Therefore, the contact current was actually approximately 6 times larger than the measured current, or > 40 nA (see PF-SECM in experimental). For a particle of approximately 3 × 10⁴ nm², this value corresponds to a current density of approximately 10² A cm⁻².

The tip-contact current observed during the SECM scan results from two sources: 1) current owing to the potential difference between the tip and the substrate; and, 2) current attributable to the reduction of Ru(NH₃)₆³⁺ in solution. The SECM tip was a Pt-coated cone approximately 250 nm in height and therefore remained exposed to the solution even when in contact with the surface.^[15] For samples in contact with an electrolyte, the reduction current measured during tip contact can thus increase relative to the current measured during lift mode and substantial tip-contact current can be present even in areas that do not contain particles.

The SECM current varied from 1.37 to 1.6 nA at 100 nm above the surface, whereas the diffusion-limited current at 1.0 μm above the surface was approximately 1.4 nA (Figure S5). The SECM currents measured above the Pt-NP/p⁺-Si surface were <1.6 nA, with the SECM current surface showing small peaks on a convoluted surface (Figure S6 and S7).

The observed tip-contact current showed a minimum value of approximately 1.3 nA, slightly less than the minimum SECM current. The approach curve data (Figure S5B) suggest that the tip-contact current for a particle-free region would show approximately 10% lower currents than the SECM current obtained 100 nm above the surface. A tip-contact current of approximately 1.3 nA is expected even in a particle-free region, in accord with observations. Moreover, all of the NPs observed in the topological scan should show a tip-contact current >1.3 nA owing to the enlarged effective tip area, again in accord with observations.

Only three particles showed a tip-contact current >1.6 nA (Figure S7), which suggested that most of the particles observed were not in electrical contact with the surface and only showed reductive current caused by diffusion in the solution. This observation is in agreement with the PFT scans in air, which indicated that only approximately half of the particles showed a contact current.

The SECM current surface had a convoluted shape that closely matched that of the tip-contact current surface (if the three large peaks are ignored; Figure S6). The similarity of the SECM and tip-contact current surfaces is expected if the source of both currents is primarily attributable to reduction of Ru(NH₃)₆³⁺. The tip-contact current for some of the particles was approximately 7 nA, for example, particle 2 in Figure 5B, which is a much larger current than that displayed by most of the other particles. In such cases, current flowing through the Si and Pt-NP to the tip contributes substantially to the total current. If the actual contact current for particle 2 is approximately 40 nA, as estimated above, then the resistance for current flow through the particle is approximately 10 M Ω , consistent with the measurements made in air.

The variation in contact and SECM currents, as well as the differences in the depressions under the particles, suggest that the electrochemical performance of electrolessly deposited Pt particles is not only the result of the uniformly low activity of all the particles, but also arises from the wide range of conductance through the particles, which allows only some of the NPs to contribute substantially to the bulk electrochemical activity of the surface.

Conclusions

Scanning probe atomic force microscopy (AFM)-based topographical, electrical, mechanical, and electrochemical measurements were used to investigate the interfaces between electrolessly deposited Pt nanoparticles (Pt-NP) and p-type Si surfaces, both ex situ in air and in situ during electrochemical reactions. Highly size-dispersed and randomly distributed particles were observed on the electrode surfaces. Approximately one third of the particles did not exhibit observable contact currents,

and another third of the particles exhibited only low contact currents. A factor of 10³ difference was observed between the contact currents of the particles in air. Local current-voltage measurements revealed a rectifying junction at the Pt-NP/p-Si interface with a local resistance $\geq 10\text{ M}\Omega$, whereas an ohmic junction with a local resistance $\geq 1\text{ M}\Omega$ was observed at the Pt-NP/p⁺-Si interface.

The electroless deposition resulted in particles that were slightly embedded into the Si. The particles were mechanically well attached to the sample surface in air, whereas the adhesion of the particles to the surface was substantially weaker in an aqueous electrolyte, and surface imaging required the use of a sub-nN force.

When Pt-NP/p⁺-Si samples in contact with an electrolyte were imaged in scanning electrochemical microscopy (SECM) mode, tip-contact currents were observed for all of the particles. However, for the majority of the particles, the current was only attributable to reduction of the redox couple in solution and not because of conduction through the Si substrate. For the particles with the highest currents, conduction through the Si dominated the current, with the particles having a resistance $\geq 10\text{ M}\Omega$. The electrical conduction through many of the particles, both in air and under the electrolyte, showed that the electrochemical performance of electrolessly deposited Pt particles was the result of: 1) many of the particles not being in electrical contact with the silicon substrate; 2) the high resistance between the NPs and the silicon substrate; and, 3) the low adhesion of Pt-NP to the Si surface. Thus, the bulk electrochemical activity of electrolessly deposited Pt-NP on Si electrodes is a consequence of the current in such devices being carried only by a fraction of the Pt particles.

Experimental Section

Materials: Boron-doped, Czochralski-grown Si wafers with resistivities, ρ , of approximately 7.5 (p-Si) and <0.005 $\Omega\text{-cm}$ (p⁺-Si) were purchased from Silicon Resource Inc. All other chemicals used were obtained commercially (see Supporting Information). H₂O with a resistivity of $\geq 18\text{ M}\Omega\text{cm}$ was obtained from a Barnstead Nanopure station (Thermo Scientific).

Fabrication of electrodes for microscopic studies: Prior to use, p-Si (111) and p⁺-Si (111) wafers were cleaved into 2.0 \times 3.0 cm or 3.8 \times 3.8 cm chips. The chips were cleaned by immersion 1) for 15 min in an RCA 1 etching solution (see Supporting Information), 2) 30 s in buffered HF(aq), and 3) 15 min in an RCA 2 solution at 75 $^{\circ}\text{C}$. The chips were then cut into 1.0 \times 1.0 cm pieces, etched in buffered HF(aq) for 30 s, rinsed in H₂O, dried with N₂(g), and immediately submerged in a Pt electroless plating solution for 45 s, followed by a thorough rinse with H₂O. The Pt electroless plating solution consisted of 1 mM H₂PtCl₆(aq) in 0.50 M HF(aq). A diamond scribe was used to scratch a Ga/In eutectic mixture (Al-drich) onto the back side of each Pt/Si chip.

Characterization of deposited Pt nanoparticles: Conductive AFM using PFT mode on a Bruker Dimension Icon atomic force microscope was used to characterize the morphology, interfacial mechanics, conductivity, and electrical properties of the electrode surfaces.^[16] Conductivity imaging during the mapping of the surface

topography was done using PpeakForce Tunneling AFM (PF-TUNA).

AFM-SECM was performed on the same Dimension Icon AFM using a PF-SECM with commercial probes obtained from Bruker. In PF-SECM, alternating line scans are run in PFT and lift modes. In lift mode, the tip does not oscillate and follows the topographical profile obtained by the previous PFT scan at a defined height above the surface. In this work, the lift height was 100 nm. The topography and conductivity of the sample were captured in PFT mode, and the electrochemical current was measured in lift mode. The currents during contact between the tip and the surface in the presence of an electrolyte were measured using a different algorithm than the contact currents measured in air by PF-TUNA (see the Supporting Information).

For the electrochemical studies, an aqueous solution of 10 mM $[\text{Ru}(\text{NH}_3)_6]^{3+}$ and 0.1 M KCl was used. A CHI760 bipotentiostat (CH Instruments, Texas) was used to control the electrochemical conditions. The electrochemical cell had a Pt wire counter electrode and a AgCl-coated AgQRE. In the SECM scan the tip was biased at -0.4 V vs. AgQRE to reduce the $[\text{Ru}(\text{NH}_3)_6]^{3+}$, whereas the sample was held at -0.1 V vs. AgQRE to reoxidize any $[\text{Ru}(\text{NH}_3)_6]^{2+}$ generated by the AFM tip.

Acknowledgements

This material is based upon work performed by the Joint Center for Artificial Photosynthesis, a DOE Energy Innovation Hub, supported through the Office of Science of the U.S. Department of Energy under Award Number DE-SC0004993. This work was additionally supported by the Gordon and Betty Moore Foundation under award GBMF1225. Research was in part carried out at the Molecular Materials Research Center of the Beckman Institute of the California Institute of Technology. J.J. and Z. H. thanks J. R. McKone, P. Núñez and R. Liu for help in sample preparation.

Conflict of interest

The authors declare no conflict of interest.

Keywords: afm · electrochemistry · energy conversion · interface · secm

[1] N. S. Lewis, *Science* **2016**, *351*, 353.

- [2] M. G. Walter, E. L. Warren, J. R. McKone, S. W. Boettcher, Q. X. Mi, E. A. Santori, N. S. Lewis, *Chem. Rev.* **2010**, *110*, 6446–6473.
- [3] M. R. Nellist, F. A. L. Laskowski, F. D. Lin, T. J. Mills, S. W. Boettcher, *Acc. Chem. Res.* **2016**, *49*, 733–740.
- [4] a) S. W. Boettcher, J. M. Spurgeon, M. C. Putnam, E. L. Warren, D. B. Turner-Evans, M. D. Kelzenberg, J. R. Maiolo, H. A. Atwater, N. S. Lewis, *Science* **2010**, *327*, 185–187; b) S. W. Boettcher, E. L. Warren, M. C. Putnam, E. A. Santori, D. Turner-Evans, M. D. Kelzenberg, M. G. Walter, J. R. McKone, B. S. Brunschwig, H. A. Atwater, N. S. Lewis, *J. Am. Chem. Soc.* **2011**, *133*, 1216–1219; c) I. Lombardi, S. Marchionna, G. Zangari, S. Pizzini, *Langmuir* **2007**, *23*, 12413–12420; d) J. R. McKone, E. L. Warren, M. J. Bierman, S. W. Boettcher, B. S. Brunschwig, N. S. Lewis, H. B. Gray, *Energy Environ. Sci.* **2011**, *4*, 3573–3583.
- [5] Bhuvana, G. U. Kulkarni, *Bull. Mater. Sci.* **2006**, *29*, 505–511.
- [6] a) D. Arrington, M. Curry, S. Street, G. Pattanaik, G. Zangari, *Electrochim. Acta* **2008**, *53*, 2644–2649; b) A. A. Amusan, B. Kalkofen, H. Gargouri, K. Wandel, C. Pinnow, M. Lisker, E. P. Burte, *J. Vac. Sci. Technol. A* **2016**, *34*, 01A126; c) J. Utsumi, K. Ide, Y. Ichiyanagi, *Jpn. J. Appl. Phys.* **2016**, *55*, 026503; d) E. Wrobel, P. Kowalik, J. Mazurkiewicz, *Microelectron. Int.* **2015**, *32*, 1–7.
- [7] J. A. Aguiar, N. C. Anderson, N. R. Neale, *J. Mater. Chem. A* **2016**, *4*, 8123–8129.
- [8] R. D. P. Gorostiza, J. Servat, F. Sanz, J. R. Morante, *J. Electrochem. Soc.* **1997**, *144*, 909–914.
- [9] S. M. Sze, K. K. Ng, *Physics of Semiconductor Devices*, 3rd ed., Wiley, Hoboken, **2007**, Chapter 3, p. 156.
- [10] Z. Huang, P. De Wolf, R. Poddar, C. Li, A. Mark, M. R. Nellist, Y. Chen, J. Jiang, G. Papastavrou, S. W. Boettcher, C. Xiang, B. S. Brunschwig, *Microworld Today* **2016**, *24*, 18–25.
- [11] R. Hunger, R. Fritsche, B. Jaeckel, W. Jaegermann, L. J. Webb, N. S. Lewis, *Phys. Rev. B* **2005**, *72*, 045317.
- [12] H. B. Michaelson, *IBM J. Res. Dev.* **1978**, *22*, 72–80.
- [13] a) R. C. Rossi, N. S. Lewis, *J. Phys. Chem. B* **2001**, *105*, 12303–12318; b) W. A. Smith, I. D. Sharp, N. C. Strandwitz, J. Bisquert, *Energy Environ. Sci.* **2015**, *8*, 2851–2862; c) F. D. Lin, S. W. Boettcher, *Nat. Mater.* **2014**, *13*, 81–86.
- [14] T. Ego, T. Hagihara, Y. Morii, N. Fukumuro, S. Yae, H. Matsuda, *ECS Trans.* **2013**, *50*, 143.
- [15] M. R. Nellist, Y. Chen, A. Mark, S. Gödrich, C. Stelling, J. Jiang, R. Poddar, C. Li, R. Kumar, G. Papastavrou, M. Retsch, B. S. Brunschwig, Z. Huang, C. Xiang, S. W. Boettcher, *Nanotechnology* **2017**, *28*, 095711.
- [16] S. B. Kaemmer, *Bruker Application Notes* **2011**, *133*, 1–12, https://www.bruker.com/fileadmin/user_upload/8-PDF-Docs/SurfaceAnalysis/AFM/ApplicationNotes/Introduction_to_Brukers_ScanAsyst_and_PeakForce_Tapping_Atomic_Force_Microscopy_Technology_AFM_AN133.pdf.

Manuscript received: May 22, 2017

Revised manuscript received: June 19, 2017

Accepted manuscript online: June 21, 2017

Version of record online: August 7, 2017